
NANOMATRIX: SCALABLE CONSTRUCTION OF CROWDED BIOLOGICAL ENVIRONMENTS

A PREPRINT

Ruwayda Alharbi¹, Ondřej Strnad¹, Tobias Klein², and Ivan Viola¹

¹King Abdullah University of Science and Technology (KAUST), Saudi Arabia. E-mails: {ruwayda.alharbi | ondrej.strnad | ivan.viola}@kaust.edu.sa.

²Nanographics. E-mail: tobias@nanographics.at.

June 8, 2022

ABSTRACT

We present a novel method for interactive construction and rendering of extremely large molecular scenes, capable of representing multiple biological cells at atomistic detail. Our method is tailored for scenes, which are procedurally constructed, based on a given set of building rules. Rendering of large scenes normally requires the entire scene available in-core, or alternatively, it requires out-of-core management to load data into the memory hierarchy as a part of the rendering loop. Instead of out-of-core memory management, we propose to procedurally *generate* the scene on-demand on the fly. The key idea is a positional- and view-dependent procedural scene-construction strategy, where only a fraction of the atomistic scene around the camera is available in the GPU memory at any given time. The atomistic detail is populated into a uniform-space partitioning using a grid that covers the entire scene. Most of the grid cells are not filled with geometry, only those are populated that are potentially seen by the camera. The atomistic detail is populated in a compute shader and its representation is connected with acceleration data structures for hardware ray-tracing of modern GPUs. Objects which are far away, where atomistic detail is not perceivable from a given viewpoint, are represented by a triangle mesh mapped with a seamless texture, generated from the rendering of geometry from atomistic detail. The algorithm consists of two pipelines, the construction-compute pipeline and the rendering pipeline, which work together to render molecular scenes at an atomistic resolution far beyond the limit of the GPU memory containing trillions of atoms. We demonstrate our technique on multiple models of SARS-CoV-2 and the red blood cell.

Keywords interactive rendering, view-guided scene construction, biological data, hardware ray tracing

1 Introduction

The cellular mesoscale describes the scales that bridge the atomistic nanoscale and the cellular microscale [1]. It starts from atoms that form larger molecules like proteins, up to the size where molecules further compose to form viruses, bacteria, or complex multi-compartmental cells. Visualizing biological structures in mesoscale helps biologists to analyze and understand the architecture and functionality of life forms. Mesoscale models of enveloped viruses reach several tens of millions of atoms in size, and these structures are just around 100 nm in diameter. Such a number only describes its macromolecular composition. If we would include water and small molecules, the number of atoms would at least double. Larger models of bacteria or complex cells reach the range of billions or trillions of atoms. *E. coli* for example contains roughly 15 billion C, N, O atoms that form its macromolecular composition. Larger structures, such as the red blood cell (RBC) consist of trillions of atoms. Each RBC consists of two-thirds of hemoglobin molecules, which are ca. 250 million in each RBC. Just the position ($3 \times \text{float}$) and rotation ($4 \times \text{float}$) information of each hemoglobin instance in a single RBC will amount to 8 GB of data in storage. Storing atomistic information about a

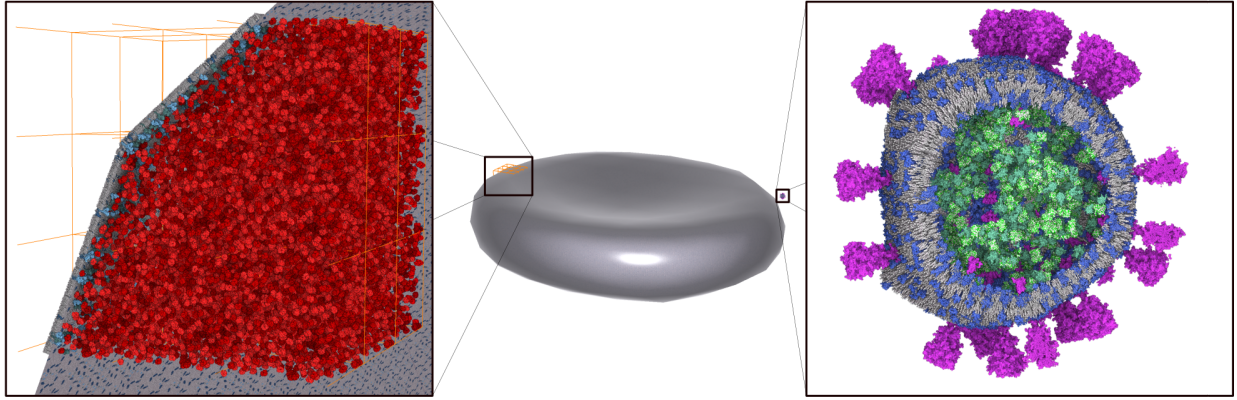


Figure 1: Red Blood Cell model of diameter 8 μm containing approx. 250 million of hemoglobin molecules, membrane proteins and lipids (approx. 335 billion atoms), with lipid-bilayer and membrane-bound proteins constructed and rendered with our view-guided two-level Nanomatrix approach. The rendering exploits hardware ray tracing, maintaining highly interactive framerates.

single RBC reaches or exceeds the limits of the memory capacity of current consumer GPUs. When attempting to store atomistic-detail information about a larger cell with 50 μm in diameter, the required memory requirement will raise to petabytes. The huge amount of data involved in mesoscale systems poses a challenge for visualization due to hardware limitations.

Current technologies are able to render biological structures up to billions of atoms. Our goal is to push this limit and effectively visualize models that contain trillions of atoms. The out-of-core approach usually renders the massive scene by keeping a fraction of data in the core memory and loading data from the disc when needed. Instead, we propose a view-guided procedural approach that generates the scene on-demand on the fly. The whole enormous scene will be never completely stored in the memory, only a fraction of it which is close to the viewer. We use a regular grid that uniformly divides the scene into cells. Only cells that are close to the viewer are populated with atomistic/nanoscale geometry, while the remaining cells use an image-based approach to depict the detail, which provides the user with a cellular/microscale description for the far structures. The main contributions include:

- For the nanoscale level, we present a new algorithm for the rapid construction of biological structures based on the Wang Tile concept.
- For the cellular level, we use an image-based Wang Tile approach, to represent the structures that are far away.
- We propose an algorithm for dynamically managing the memory to change between the atomistic and cellular representations.
- We propose a parallel rendering scheme that utilizes hardware-accelerated raytracing for molecular visualization.

2 Related Work

Large-scale Molecular Visualization: There is a variety of tools for molecular visualization, such as VMD [2], Mol* [3], or PyMOL [4]. These tools have been designed for molecules with up to thousands of atoms and are not suited when the data size exceeds tens of millions of atoms [5]. Similarly, generic visualization tools like Amira [6] prioritize generality over scalability and thus reach their limits with increasing dataset sizes. Waltemate et al. [7] map lipid bilayers onto a mesh geometry with interactive rendering performance for up to 10 million atoms on NVIDIA GeForce GTX 770. Megamol [8] is a visualization framework designed to address interactive visualization of large particle-based datasets. The system is able to render up to 100 million atoms at interactive framerates, which represents in biology scale a virus or a small bacterium. Recently, Ibrahim et al. [9] introduce a probabilistic occlusion culling architecture using meshlets for acceleration. The algorithm was able to render 232 million particles in 41 frames per second (FPS) on an NVIDIA RTX Titan 24GB. Lindow et al. [10] have first presented interactive visualization of large-scale biological data that consists of several billions of atoms. As the biological models often consist of a large number of recurring molecules of a few number of proteins, they create for each protein a 3D grid structure containing all its atoms and store the grid on the GPU as a 3D voxel and then utilize instancing to repeat the proteins in the scene. In the rendering stage, they draw the instances' voxel and perform raycasting in the fragment shader. Their method was

able to render 4,025 microtubules with approximately 10 billion atoms with at least 3 FPS on a NVIDIA GTX 285. Falk et al. [11] extend this work by optimizing the depth culling and the rendering method and they add an implicit Level of Detail (LoD) approach. They were able to render 25 billions atoms in 3.6 FPS using a NVIDIA GTX 580.

Le Muzic et al. [12], introduced an optimized approach using a straightforward LoD scheme that does not require grid-based supporting structures. Instead, it relies on the tessellation shader to dynamically inject sphere primitives in the rasterization pipeline for each molecule instance. Later, they extend this work and introduced cellVIEW [13] where they reduce the number of injected sphere primitives into the rendering pipeline. The cellVIEW system has set a benchmark with its ability to render 250 copies of a HIV virus model in blood plasma at 60 FPS on NVIDIA GTX Titan. This scene contains 16 billion atoms (each replica contains around 64 million of atoms). The goal of our proposed approach is to push this limit and visualize a large biological model that contains trillions of atoms. All of the above mentioned techniques use procedural impostors for representing atoms to simplify the geometry and accelerate the rendering [14, 15].

Procedural Modeling: Generating 3D digital content is a very time consuming and tedious task, while many environments contain self-similar and repetitive structures [16]. Procedural modeling techniques offer a way to create 3D models from sets of rules or algorithms. Very early approaches like L-systems use formal grammars to describe natural patterns as they appear in trees, for instance. Other phenomena like fire, water, gases, and clouds have also been procedurally generated for decades. In recent time, computer graphics has experienced significant advances in the procedural modeling of natural as well as man-made structures. Computer games and movies utilize procedural modeling techniques to create large worlds with varying shapes and styles. A fundamental part of such worlds is the automatic modeling of architectures [17] with different building designs. Such techniques are capable of generating infinite cities [18] or rich forest scenes [19] in real-time. In order to generate detailed content in real-time, the research focus has shifted towards parallelization [20, 21], such that computation and memory can be efficiently mapped on graphics hardware. While most procedural modeling techniques target open worlds, in this work, we focus on a very constrained space where the content is defined through scientific measurements. Procedural modeling in mesoscale environment is a challenging task. This environment is highly dense with heterogeneous molecular structures in size and shape. There are several modeling techniques that target molecular landscapes, one of which is CellPaint [22]. CellPaint allows users to create dynamic molecular illustrations using a 2D style, which shows a cross-section of a biological mesoscale scene. Mesocraft [23] allows the user to interactively specify a set of rules that define the spatial relations of the model's molecules and propagate these rules through the model which results in rapid modeling. Mesocraft and CellPaint are semi-automatic modeling techniques where the user is expected to participate in the building process of the biological structure, for example, changing the position of a molecule or rotating it. In contrast, our construction approach is fully automatic. Once the user provides the algorithm with the required input, the model is generated without any user interaction.

Atomistic modeling in mesoscale environments is typically based on packing algorithms, as demonstrated with cellPACK [24]. Packing molecules is a computationally demanding task. Assembling a 3D mesoscale model from scratch via cellPACK could take from minutes to hours, depending on the size and complexity of the model. Klein et al. [25, 26] propose the *instant construction* approach to rapidly create mesoscale models. It consists of a set of GPU-based population algorithms which generate different types of biological structures. Similarly, we present a GPU-based population algorithm; however, our approach differs in several aspects. First, the *instant construction* algorithm for populating the membranes required the mesh to be defined as an equally-sized quad-based surface to place the Wang tile on these quads while our method uses the texture coordinates to map the tile into the triangle mesh of varying size directly. Second, they populate the soluble proteins randomly and then resolve the collisions using a force-based approach while we use the collision-free tile cubes to populate the soluble proteins, which eliminates the need for collision handling and subsequently decreases the population cost.

Texture Synthesis: Our approach of generating patches of geometry is very related to the synthesis of textures, especially in the context of Wang Tiles. Originally, the Wang Tiling concept [27] has been proposed as a formal system to cover an infinite plane with non-periodic patterns from a small set of tiles. The concept is based on tiles with color-encoded edges, whereas each tile is arranged in a way that its edge color matches the adjacent neighbor. Later adaptions of this approach have been used to map 2D textures onto 3D geometry. Fu and Leung [28] have extended the concept to apply Wang Tiles on arbitrary topological surfaces. Li-Yi [29] avoid storing large textures on graphics processors by presenting a Wang Tiles-based texture mapping algorithm that generates large virtual textures directly on GPUs through a fragment program. Culík and Kari [30] introduce Wang cubes with color-encoded faces which is a generalization of Wang Tiles in 3D. Doškář et al. [31] use Wang cubes to generate compressed representations of complex microstructural geometries. Considering that such approaches are constrained to map color information to tiles, in this work we target to map geometry to tiles. The major challenge of the application of Wang Tiles lies in the

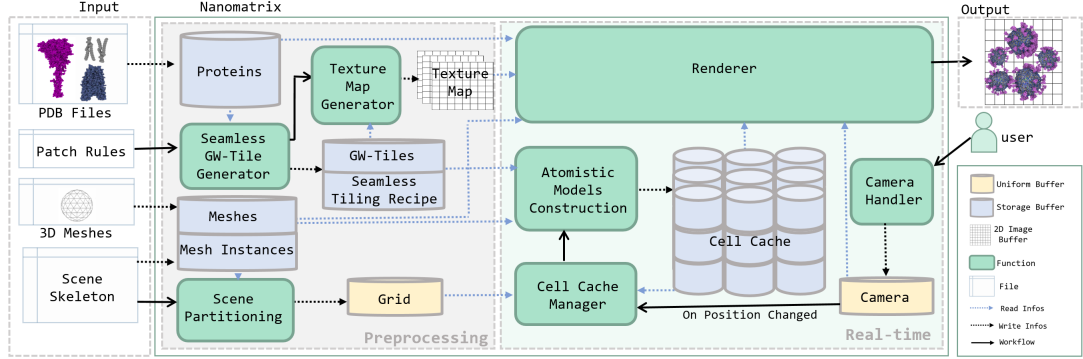


Figure 2: Nanomatrix – the scalable construction algorithm. Based on the input structure and building rules, in the preprocessing step rectangular geometry based or image based aperiodic patches are generated. For representing a volume of molecules, box tiles are generated. In the real-time rendering, these tiles populate the scene with the appropriate level of detail depending on the distance from the camera. The scene is then rendered using RTX ray tracing so that the population and rendering fully utilize separate computational units on the graphics hardware.

generation of the tiles, as well as handling the issue of overlapping geometry in the 3D case. Comparable approaches with geometry lack performance or use regular patterns [32].

Parallel Rendering: Parallel rendering aims to improve the frame rate by dividing the workload between multiple renderers. Generally, two of the three rendering architectures classified by Molnar et al. [33] have taken the most attention. The first category, so called *sort-first*, involves dividing the screen into disjoint regions and each renderer is responsible for all computations that are related to its region. Each renderer accesses its own copy of the scene, making memory management inefficient. Another rendering architecture category, so called *sort-last*, divides the scene’s primitives rather than the screen. Renderers compute a full-screen image of their portion of the primitives then submit these pixels to compositing processors that sort the rendered images in visibility order to produce the final image. This method can result in a very high data rate as the renderers operate independently until the compositing step. The *sort-last* strategy is suitable for applications that require interactive, high-quality rendering and efficient memory management. For more details, we refer the reader to [33–35]. Our rendering algorithm uses the *sort-last* approach.

Zellmann et al. [36] investigated how data could be efficiently partitioned across the parallel GPUs using a ray tracing-based renderer. They define the properties of a good primitives partitioning; first, even data distribution, to make good use of the GPU memory and compute resources. Second, even spatial distribution because irregular spatial distribution may cause load imbalance and subsequently inadequate rendering performance. In addition, minimal object overlap and replication because in those two cases, the ray tracer would intersect the primitive more than once. Our method uses a spatial partitioning scheme to distribute space equally among cells. Each primitive in the scene belongs to only one cell, so no primitive is replicated. Parallel rendering usually utilizes multiple GPUs to accelerate the rendering; however, our rendering algorithm is executed in a single GPU that runs multiple rendering threads in parallel through a compute shader.

Out-of-core Scientific Visualization: When the dataset is too massive to fit inside the internal memory, it becomes important to manage the memory space effectively. Out-of-core techniques store only a small fraction of the data in the fast internal memory and keep the remaining part in the slower external memory. Varadhan and Manocha [37] use a graph structure to represent the scene where each node in the graph is associated with a precomputed LoD of the objects. At run-time, they use occlusion culling to load only visible objects from the external memory. Funkhouser [38] introduces an algorithm that predicts the possible viewpoint locations in the next frames and uses that information to determine a set of objects that would be soon visible. Fraedrich et al. [39] propose a GPU-accelerated visualization algorithm that minimizes the number of particles-data to be streamed from disk to the graphics subsystem. They construct an out-of-core adaptive octree and use it as LoD particle representation. At its finest level, the octree has a resolution sufficient to represent all particles individually. Rendering is then performed using the octree level that has cells just higher than screen resolution to minimize error. Their system was able to render 10 billion particles at different scales on 11 FPS. Wald et al. [40] introduce a framework that allows interactive ray tracing of massive amounts of geometry by using an out-of-core demand-loading and memory management scheme. The input/output communication between the internal and external memory is the bottleneck of the out-of-core approach. Vitter [41] provides a survey of the algorithms and data structures that have been proposed to optimize fetching the needed data from the external memory and reduce the I/O cost. In this paper, we are using an exclusive in-core approach and trade

memory with compute. Instead of fetching the data from external memory, we construct it on the fly when it is needed. Beyer et al. [42] employ the concept of distributed shared virtual memory and use the *sort-last* approach to distribute the rendering task between multiple GPUs. The huge 3D volume is represented as a virtual regular grid. The volume is virtual because the data are only created on-demand when it is located inside the view frustum either by fetching it from the disk or reconstructed on the fly. The grid cells are arranged in each node so that only ones that intersect the view frustum are rendered.

3 Technical Overview

None of the currently available visualization methods is able to visualize large macro-molecular structures such as the red blood cell (RBC) in full atomistic detail or multiple instances of viral and bacterial ultrastructures. These structures are simply too large to fit into the CPU and/or GPU memory along with associated acceleration structures. At the same time, at any moment, only a small fraction of such a huge dataset can be seen. Therefore, a natural memory-saving and acceleration strategy is to store only those parts of the model in the memory that are visible from the current viewpoint. One solution is to use an out-of-core approach and stream the model from the disk to the core memory. However, instead, we are using an exclusive in-core approach and generate the model on-the-fly, where the camera triggers the process of generation. Our approach operates under the following condition: Biological structures that are far away are enclosed by their molecular envelope, such as a lipid bilayer for example. Far away structures are never cut open or clipped in the middle, this happens only when the camera is close to a particular structure, only then the envelope can open to see the atomistic detail inside.

Before we dive into technical detail, we clarify the terminology of the individual components involved in our approach (Figure 2). Our Nanomatrix approach generates geometry at atomistic detail of the *potentially visible* portions of the view. By *potentially visible* we mean structures that are either (1) close to the camera, so that the atomistic detail becomes discernible or (2) there is a clear view of these structures unobstructed by other densely packed molecules. Our approach also generates image texture representation for those structures that are potentially visible but are so far away from the camera that their atomistic detail is no longer perceivable. To realize this, four elements are expected as input. First, the structure of all types of molecules that will be populated in the scene is stored in **PDB files**. These files are available at the *Protein Data Bank* (wwpdb.org). The second input type is the **3D patch rules**, where the **3D patch** is a small, collision-free 3D biological model that is constructed based on its **rules**, which define the concentration of various molecules in the patch and the principles that spatially characterize their spatial relations. Our approach uses two types of patches: the **rectangle-based patch** and **box-based patch**, both are illustrated in Figure 3. The third input is the **3D mesh** which defines the geometry of a given biological compartment. The scene may contain several copies of the same biological structure, the information that is needed to instantiate the given meshes is given in the **scene skeleton** file.

Once the input files are given, the pre-processing phase starts preparing the necessary components for the construction and rendering phases. As we aim to visualize models that do not fit into the memory, we need to partition the space and keep only potentially visible parts of the scene in the memory. The **scene partitioning** divides the 3D space into small non-overlapping **cells** of identical sizes, along each axis that all together form the regular **scene grid**. Unless explicitly stated in the remainder of the paper, we refer to the **cells** as the elements of the scene grid as a technical term. Our visualization is concerned with biological cells, but if this term occurs in that context, it will be explicitly denoted as being a *biological cell*. Also, the **cell** is an element of global scene partitioning, in contrast to the **box** or **rectangle tiles**, which are elements forming the detail of a particular biological entity. Each cell is associated with an **index** which defines the cell location (i, j, k) within the grid. At any moment, only a small group of cells will be populated. We call this group of cells the **active cells**. To identify them, the camera's location within the grid is obtained first, which represents the **central cell**. This cell, together with its neighboring cells, represents the active cells. The number of the active cells depends on the size of **activation window**, which indicates the number of central cell's neighbors that should be considered active. Each active cell points to a **cell cache** which is a GPU storage buffer that is readily available to be filled with geometric instances forming the structural information of a biological entity.

The proposed construction approach uses the *Wang Tiles* concept for populating the cells. We introduce a novel concept of aperiodic geometric tiles, denoted as *Geometric Wang Tiles* or **GW-tiles** for short. These tiles are generated from a larger 3D patch as described in Klein et al. [26], so that the GW-tiles can be arranged to form a seamless tiling. In the pre-processing step, a description of such arrangement is created and denoted as **seamless tiling recipe**. This recipe is described in a 2D table of pointers that refer to one of the generated GW-tiles.

For structures that are far away from the camera that cannot be observed closely, the detail is represented by an image texture, instead of a geometry texture. Therefore, once a GW-tile is obtained, its geometry is used to generate the

texture map, which is composed of diffuse, normal, and ambient occlusion seamless textures. The texture map can be used in the deferred shading step when mapped on a mesh.

During the rendering, when the camera moves to a new location, the **cell cache manager** will update the active cells, as well as the pointers to the cell cache, and then submit the cells that need to be generated to the **atomistic models construction**. This procedure populates the proteins in the cells using GW-tiles and seamless tiling recipe. The constructed scene is rendered in two passes. In the first pass, each active cell computes a full-screen image of their portion of the atomistic models using hardware-accelerated ray tracing that is available on GPUs. The resulted images are then composited in the second render pass to form the final rendered image. During the compositing render pass, if the ray hits an atom in one of the active cells' image buffers, the closest hit is used to assign the final color and the ambient occlusion value is computed. Otherwise, the *texture map* is used to texture the scene mesh.

4 Pre-processing Phase

Before the real-time rendering, in the pre-processing step, we partition the scene, fill the scene with mesh instances. We also prepare the geometry for all meshes, prepare and upload buffered data to the GPU.

4.1 Scene partitioning

The entire scene will be partitioned into several cells which will be during real-time rendering filled with structures on demand. These cells are organized in a grid that covers the entire scene. To create the grid, the first task is to define the axis-aligned bounding box (AABB) that tightly encloses the object distribution in the scene. These objects represent biological structures, such as biological cells, viral particles, bacteria, or organelles, which come in different sizes, and shapes. We use 3D mesh to define their boundaries that separate the internal parts of these structures from the outside environment. As the scene may consist of several copies of the same structure, the scene skeleton file contains information needed to instantiate the given meshes in the scene. This file contains a list of mesh instances and for each instance, the *mesh-id*, *patch-id*, *position*, and *rotation* are provided. The meshes and scene's skeleton are together used to estimate the scene's grid AABB.

The scene space is uniformly partitioned into a set of non-overlapping 3D cells of identical extents. The resulting regular grid is defined by the number of cells along every axis that represent the grid dimensions *grid.dim*, and by the size of the cell *cell.size_{xyz}*. In this 3D grid system, a cell is indexed by column (*i*), row (*j*), and layer (*k*) which represent the cell location in the grid. Thanks to the regularity of the grid, we do not build any kind of explicit data structure for the scene cells. All needed positional information can be obtained from the above defined quantities. We define our very first cell, indexed with (0, 0, 0) having its center in the origin of the so called *grid space*. An offset *grid.min* can be used for calculating the position of the minimal cell corner *cell.min_{xyz}*:

$$grid.min_{xyz} = \frac{-1 \times cell.size_{xyz} \times grid.dim_{ijk}}{2} \quad (1)$$

$$cell.min_{xyz} = (cell_{ijk} \times cell.size_{xyz}) + grid.min_{xyz} \quad (2)$$

In addition, we can easily access to a cell *cell_{ijk}* that corresponds to a particular 3D position *P_{xyz}*, or calculate the cell center *cell_{xyz}* by the following two equations:

$$cell_{ijk} = \lfloor \frac{P_{xyz} - grid.min_{xyz}}{cell.size_{xyz}} \rfloor \quad (3)$$

$$cell_{xyz} = cell.min_{xyz} + \frac{cell.size_{xyz}}{2} \quad (4)$$

4.2 Tiles Preparation

Our strategy for filling a certain 3D volume with particular molecular instances is by filling it with a limited collision-free set of 3D tiles [43] that are prepared and stored during the pre-processing step, intended for use during the real-time rendering. With such a construction approach, we overcome the computational load needed for populating huge amounts of elements on-the-fly. Moreover, this construction minimizes the collisions of populated elements.

First, a 3D patch populated with molecules is generated. For this purpose, we use the MesoCraft tool that was designed for generating biological assemblies based on the simple geometrical rules that define relations between elements, molecular structures in our case [44]. The rules description is out of the scope of this paper, however, it is important to

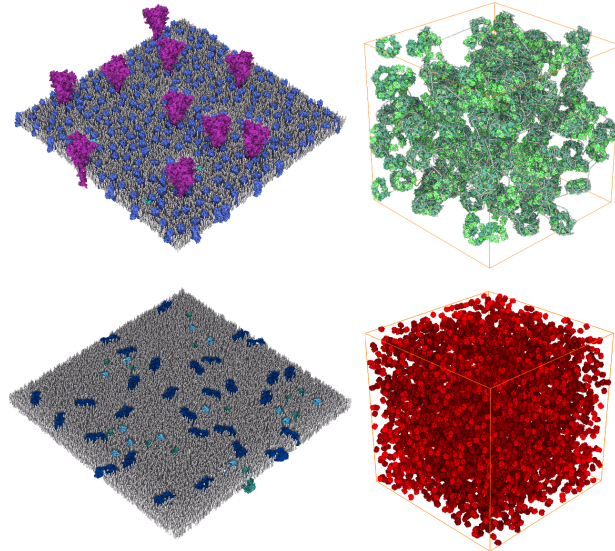


Figure 3: Illustration of rectangle-based patch (l) and box-based patch (r) for SARS-CoV-2 (top row) and RBC (bottom row).

mention that MesoCraft integrates the collision handling algorithm. Therefore, the resulting patch can be collision-free. We work with two different patches; rectangle-based and box-based. A rectangle-based patch is formed by molecular geometry populated on a rectangle. The molecular distribution is with a reference to a plane and is later used for populating a membrane. The second type, a box-based patch, is formed by populating molecular geometry inside a box (distribution in a unit of volume) and is typically used for populating soluble proteins inside structures. The comparison of both types can be seen in Figure 3. We create box patches with the dimension of $100 \times 100 \times 100$ nm filled by 1,000 protein structures. After replicating several instances next to each other, our experiments show that the seams, resulting from periodic tiling, are not noticeable for box tiling. The reason is that this tiling is only used for filling an internal part of a biological structure. After the camera penetrates inside the structure, due to the densely populated environment, the user is immersed among multiple structures, which leaves a limited possibility to identify the seams. Therefore, we do not additionally process these box-shaped patches. Rectangle-based patches form membranes that the user can see from the outside. For this reason, the rectangle-based patches need to be processed further, to guarantee a seamless geometry, see below.

To generate seamless *geometry textures*, we implemented the Wang Tiles concept that works with 16 base tiles. The process is illustrated in Figure 4. From the geometry rectangle-based patch that is collision free (see Figure 3 (left)), four initial non-overlapping base patches B are randomly selected and each of them is associated with a color. From the base patches, a set of tiles L using the Wang Tiles approach is created in the following way. Every base patch from B is subdivided into four triangular sub-patches. A tile $l \in L$ is created by combining four triangular sub-patches from any of B to form a rectangle. Therefore, the collisions need to be solved if two neighboring triangular sub-patches come from different base patches. We work with basic 16 configurations of tiles (can be seen in detail in Figure 4). However, more configurations can be taken into account. The more configurations are used, the even bigger diversity of the generated result. Later in the population phase, if two tiles are laid next to each other so that the triangular sub-patches on both sides of the shared edge are from the same base patch (are associated with the same color), they do not create a seam and there is no need to solve the collision.

After the tile-set L is created, for every molecular instance $m_i \in l$, where $l \in L$, its uv -texture coordinate $uv(m_i)$ within the rectangular tile l is computed. This coordinate is within $[0, 1]$ space and we call it the *tile texture coordinates*. From tile set L we later generate a *tile recipe* TR that is associated with one of the meshes in the scene. A *tile recipe* is a 2D array that contains indices of tiles from L (a value from the range $[0..15]$) and represents a lookup table when texturing or populating the respective part of the mesh during real-time rendering.

Scene structures can be viewed from a large distance, where the atomistic detail would gradually result in seeing variations of colors on a mesh surface, instead of recognizing any detailed geometry. Therefore, when the biological entity is far away, it is covered with an image texture instead of a GW-tile. However, we need to maintain correspondence between GW-tiles and the texture map. When zooming in, the rendering algorithm combines the texture mapping with atomistic detail and blends between them. To reduce the additional handling overhead during rendering, we create a

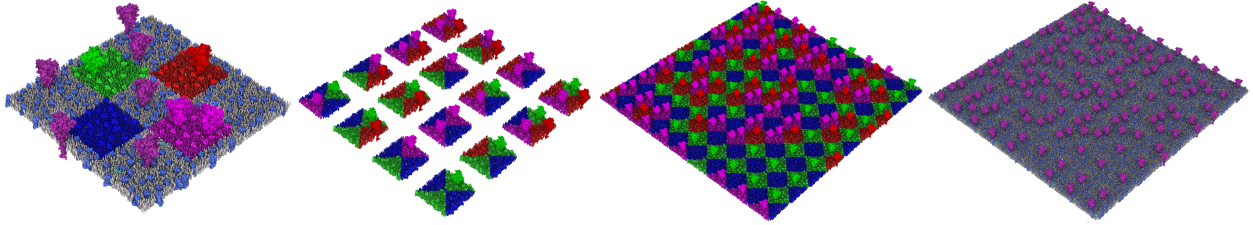


Figure 4: Illustration of the tiling algorithm. From left: four randomly chosen initial patches inside rule-based geometry patch, 16 base Wang Tiles, population of the tiles using a tile recipe rendered with and without Wang Tiles encoding.

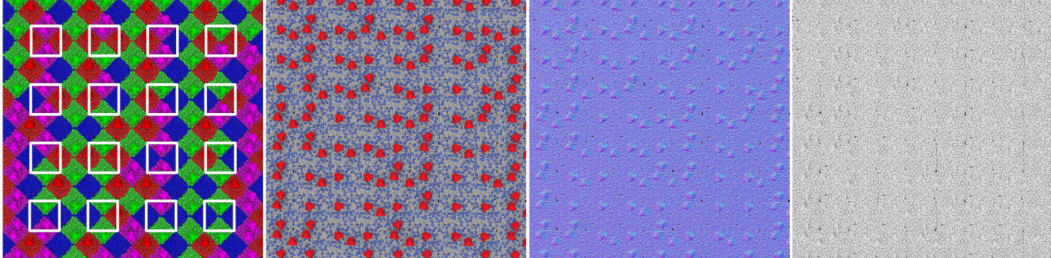


Figure 5: Illustration of the textures obtained from the geometry tiles. From the left: texture generated by Wang tiling with highlighted 16 base tiles; Diffuse texture; Normal texture, Ambient-Occlusion texture.

single texture that contains all the tiles. Importantly, we need to correctly sample the values at the border of the tiles, which implies a special construction of the texture map.

We create a single texture map directly out of the GW-tiles. The texture map is not used in its continuum for texturing, it rather contains 16 texture tiles for sampling, with a space between these tiles to secure correct sampling on the border of each tile. We render a geometry patch from the top view along the y -axis such that the patch is aligned with the xz -plane. This patch consists overall of 9×9 GW-tiles which are placed in a seamless way between them. However, for sampling the texture map later in the real-time rendering stage, we only need 16 tiles depicted in Figure 5. The texture map is generated as follows: All 16 GW-tiles are positioned by facing the y -axis into four rows and four columns with a gap between the tiles of the size of one tile in both x and z directions. Then, those gaps are filled in the first iteration in x direction and in the second iteration in z direction to complete a seamless Wang Tile pattern. In the last iteration, a set of tiles is placed to create a border enclosing the previously placed tiles. Such a structure allows us to easily identify the coordinates of individual 16 base tiles, which we use for sampling, based on their indices. For example, if the resulting texture map is rendered with the resolution of 1800×1800 pixels (meaning one tile is 200×200 pixels as this is 9×9 grid), for example, the square in the texture representing the tile with index 6 is $[600, 1000, 200, 200]$ (top, left, width, height).

5 Cell Cache Management

Only a portion of the scene geometry content is available in the memory at any given time during the real-time rendering stage. We achieve this using uniform space partitioning into cells. Next, we need to identify which cells among the scene's cells should be visualized and stored in the memory. We denote this scene's cells as the *active cells*.

In our viewpoint-guided approach, the camera position is used to identify which cells should be active. Therefore, we first define the *central active cell*, which is the cell enclosing the camera. It can be obtained using Equation 3, where P_{xyz} is the camera viewpoint. After the central cell is identified, the neighboring cells are obtained. Thanks to the regularity of the grid, the adjacent cells of the central cell are easy to locate. In our implementation, we activate only the closest neighbor to the central cell in each axis i , j , and k , so the size of our *activation window* is $(3 \times 3 \times 3)$ which gives us 27 active cells C . However, based on the computational resources and settings of the size of the cells, this can be set to a larger number. Increasing the size of the activation window will increase the rendering overhead because each cell is drawn in a separate draw call, thus a larger number of images will need to be rendered for the final scene compositing.

The size of the activation window specifies the number of cells that will be populated and rendered. Subsequently, it specifies the number of *cell cache buffers* that need to be prepared. The *cell cache* is a GPU storage buffer that is readily

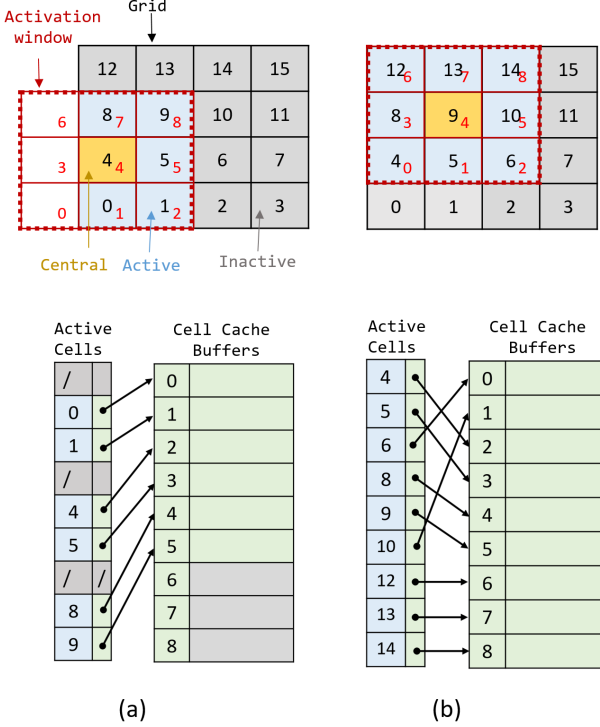


Figure 6: Illustrating the indexing-based algorithm for cache buffers dynamic allocation. In this 2D example, the scene grid contains 16 cells and the number of active cells is 9. (a) and (b) show two different central cells, where in each case the central cell is highlighted with the yellow color, while the active cells with blue color.

available for the active cell to be filled with populated instances. This memory buffer is pre-allocated to fit a relatively large number of instances. In the prepossessing step, we allocate 27 storage buffers that represent the cell cache. As our scene is continuously regenerated, we choose to allocate cell cache in advance and just fill and clear them in real-time to avoid the overhead that comes from the frequent memory allocation and deallocation.

The cache manager controls the process of reusing deactivated cells by updating the pointers between the cell cache buffers and active cells and triggers an event that leads to the regeneration of the scene inside newly active cells. Figure 6 shows an example that illustrates this algorithm on a 2D grid. In this 2D example, the scene's grid contains 16 cells and the size of the activation window is 3×3 . In Figure 6 (a), the camera is located in cell 4, which becomes the central cell and the cells 0, 1, 4, 5, 8 and 9 are the neighbors and all of them are inside the activation window. These cells are the active ones and should be populated. Every active cell should occupy a cell cache to fill it later with molecular instances in the construction stage. Once a cell becomes active, an unoccupied cell cache will be reserved for this cell and a pointer will be created to link them. This cell will be added to the list of cells that will be submitted to the construction stage. If the camera moves to the cell 9 as shown in Figure 6 (b), the cells 6, 10, 12, 13, and 14 entered the activation window and need to be constructed while the cells 0 and 1 left the activation window, therefore, their pointers to the cell cache have been deleted. This makes these cache buffers available for other cells. Cells 4, 5, 8, and 9 were populated previously, and they are still pointing to the same previous cell cache buffers. These pointer operations are important to avoid copying between buffers. In other words, if a cache has been assigned to a cell, it will be reserved for that cell as long as the cell is inside the activation window.

6 Atomistic Models Construction

In the pre-preprocessing phase, both rectangular-based and box-based geometry tiles are prepared. For their population, we implemented two distinct population methods. The first method is designed for the membrane population using rectangular tiles, the second one for the population of the inner matrix of the biological compartment using the box tiles. Both methods are described in this section.

A biological membrane of a virion or a cell is typically a thin envelope that consists of lipid bilayer and membrane-bound proteins. Because the membrane is targeted to be visible from a distance, it has to appear seamless so the observer cannot notice any artifacts caused by repetitive patterns. For the box-based geometry tile, while the viewers observe the inner part of the models, they are immersed in a heavily populated environment, where spotting any repetitive patterns is highly unlikely. For representing an overall shape of the virion, we use a geometry mesh that can be created by 3D modeling tools or directly derived from biological measurements. In the following, an algorithm that populates molecular instances along the mesh is described.

6.1 Input Preparation

In the pre-processing phase, we describe how the geometry tile set L is prepared. The tiles set consists of rectangular patches containing molecular instances where every molecular instance is assigned its tile texture coordinate within the range $[0, 1]$ with respect to the rectangle. For performance reasons in the population phase, there are many threads that populate the structure in parallel. A single population thread is responsible for processing a single molecular instance per triangle, in case of rectangular tiling, and per cell, in case of a box tiling. We need to find a conservative estimate of threads to initialize before executing the population process. For that we identify a tile containing the maximal number of molecular instances and store this maximal number in $tileL_{max}$ or $tileB_{max}$, depending on whether it is a rectangular or a box tile. Then, in rectangular tiling case, we identify how many tiles are needed for covering the largest triangle in the scene. The total number of threads allocated for tiling each triangle is then the product of the number of instances in $tileL_{max}$ and the number of tiles necessary for tiling the largest triangle in the scene. For the box tiling, we allocate the number of threads analogously, i.e., the number of instances in the box tile $tileB_{max}$ is multiplied by the number of tiles necessary for filling one entire cell.

Another required input is a triangular mesh, where every triangle is associated with the texture coordinates as well. We expect that the mesh already contains texture parameterization and both *mesh uv-texture coordinates* are within $[0, 1]$ range. The algorithm uses the texture coordinates for transforming molecular elements from mesh texture coordinates to tile texture coordinates and vice versa. If the mesh does not have a texture parameterization, a simple cube-map or spherical texture parameterization can be applied and used. However, depending on the shape of the mesh, it might be non-trivial to create fully seamless texturing. A seam in texture parameterization would result in a visible seam. The scene can contain multiple different meshes. For simplicity, in the rest of the paper, we refer to a single mesh. However, the method works in the same way for every mesh that has a texture parameterization.

Our goal is to populate rectangular tiles over a mesh so it forms a continuous surface. These tiles can be represented either by geometric molecular instances or by the corresponding image texture. Therefore, we need to establish a mapping from the mesh texture coordinate system into the tile texture coordinate system and vice versa. After that, we compute a size of the grid formed by tiles from tile set L that cover the largest triangle of the mesh. This grid is later used to populate tiles on all mesh triangles. The largest triangle t_{big} within the set of triangles T is identified. As all the tiles in L are of the same size, the ratio between the size of t_{big} and one representative tile $tile$ is computed. The ratio represents the number of tiles (rep_u, rep_v) needed for tiling to cover the entire area of triangle t_{big} with a sequence of tiles in its plane. Moreover, a mapping $tile_{uvsizes} = (uvmax(t_{big}) - uvmin(t_{big}) / (rep_u, rep_v))$ that represents the size of the tile in the texture coordinate space associated with the mesh, is computed.

For the entire mesh, a tiles recipe TR using Wang tiling approach is created. The resulting size of the tiles recipe, which is in fact a 2D array, is computed as $(1/tile_{uvsizes})$. Afterwards, the array is filled with the indices of tiles from L by the Wang tiling generator. This structure is prepared for later sampling for determining a tile at an arbitrary texture coordinate that belongs to the mesh. By dividing a uv mesh texture coordinate by $tile_{uvsizes}$, we get two-dimensional index into TR . The other way around, if we multiply TR by $tile_{uvsizes}$, we get the size of the mesh texture. To this point, previously described computations are performed only once. The description of the iterative algorithm that populates a grid of active cells C follows.

We need to populate the rectangular tiles on the mesh. As the mesh can be of arbitrary size, we constrain the population by the grid of active cells C . The active cells can be in three configurations: outside of a mesh, inside of a mesh, or intersecting a mesh. First, we initialize $c.cache$ for every $c \in C$ to void values. No information about any molecular instance nor intersected triangles of a mesh are stored. The $c.closestTriangle$ variable representing the closest triangle of a mesh to c is set to null. This initialization is later done for new cells that are added into the set of active cells C . Next step is to compute a set of intersected triangles I_c (where $I_c \subset T$) for every $c \in C$. This information is stored for the particular cell in $c.cache$. Furthermore, for those active cells c that are entirely inside or entirely outside the mesh, we need an in-out test. To achieve this, we store a reference to the closest triangle to such cell c from all triangles I_c : $c.closestTriangle = closest(\forall I_c)$. The in-out test is described in subsection 6.3.

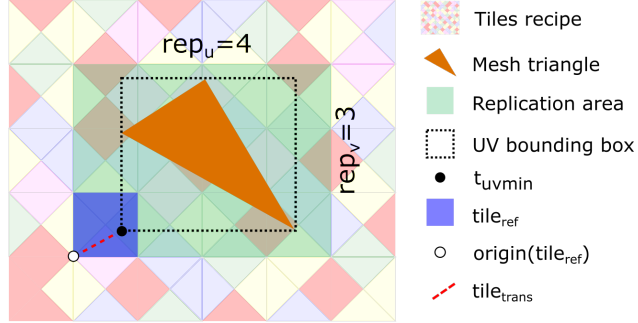


Figure 7: Projecting a mesh triangle to the tiles recipe. The position of t_{uvmmin} determines the reference tile $tile_{ref}$ from the tiles recipe TR . Based on the size of the triangle, the amount of tiles (rep_u , rep_v) needed to cover the triangle is estimated. The offset $tile_{trans}$ in the mesh texture coordinates refers to the vector from t_{uvmmin} to the origin of the reference tile $origin(tile_{ref})$.

6.2 Membrane Population

To populate the membrane, we cover the mesh of a biological structure with a rectangular grid based on its texture parameterization. Each element of this grid represents a single tile from the tiles recipe TR associated with the mesh. Our approach is to align each triangle of the mesh with a plane of the TR grid. Based on the texture coordinates we obtain a sub-grid that encloses the triangle and then re-project the sub-grid with its respective tiles onto the triangle in the 3D space. This way we obtain the 3D position of the starting corner of the sub-grid and also its orientation in world coordinates. Within this sub-grid we populate all molecular instances in parallel. In our case, the sub-grid has always the same dimensions (rep_u , rep_v) calculated from the biggest triangle of the mesh and we use it for smaller triangles as well. The sub-grid completely covers the triangle area, but tiles can also lie outside the triangle t area or outside the cell c . Overall, we run for the sub-grid $tileL_{max} \times rep_u \times rep_v$ threads. Threads are associated with a particular molecular instance m that belongs to a certain $tile$ and is stored in a linear buffer. Few remaining threads that exceed the number of molecular instances for a particular tile are discontinued. The molecular instance m is associated with a tile l is indexed by two indices in the 2D array of the sub-grid. To correctly define the 3D position of the molecular instance $m.pos$, we need to calculate it as a position within its tile l and add the 3D position of the starting corner of the l . The 3D position of the starting corner of l can be calculated based on l indices within the sub-grid and the tile extents in the world coordinates in both dimensions. The calculation of position is analogous to indexing in multidimensional arrays. The only step is to determine the 3D position of the starting corner of the sub-grid $origin(tile_{ref})$ (as shown in Figure 7). This 3D position we obtain from the known world-space 3D position corresponding to t_{uvmmin} and the known world-space offset $tile_{trans}$. Afterwards, we crop all the instances that lie outside of the triangle (using barycentric coordinates of the instance) and outside of the cell c . If the position pos passes the criteria, the $atomicCounter$ is increased and a new molecular instance m is recorded in $c.cache[atomicCounter] = m$. Its type is set according to $m.type = m_{ref}.type$ and the position is set to $m.pos = pos$. The rotation is stored in an analogous way. The only difference with the rotation is, that it has to be adjusted by a rotation representing the rotation around the y -axis into the normal vector of the triangle. The y -axis is used as all the tiles were generated with the default orientation facing the y -axis.

6.3 Solubles Population

In the previous section, the description of membrane population was discussed. The next step is to populate internal parts of the biological structures with molecular instances, not the external space on the other side of the boundary. Similar to the membrane population, this approach is based on tiles. However, instead of the rectangular-based tile-set L , the box-based tile-set B (see Figure 3) is used. In this case, population does not rely on the texture coordinates of the mesh. Moreover, there is no Wang Tiles approach used for the B tile-set. As these are not visible from outside the structure and when immersed inside, it is very unlikely to notice any seams in such a crowded environment. Therefore the seamless constraint is not applied in the box-tiling case. In principle, the same Wang Tiles concept as previously explained can be extended to 3D and used for B tiles. In our implementation we generate each box tile $b \in B$ using the same size $size(b)$, limited to the cell $c.size$.

The population is done for every cell c independently. Firstly, as previously mentioned, intersected triangles for every $c \in I_c$ are computed. Moreover, a list of intersected meshes I_{meshes} specifying into which meshes the triangles I_c belong is created. Afterwards, $c.closestTriangle$ (see subsection 6.1) is determined. Every mesh is associated

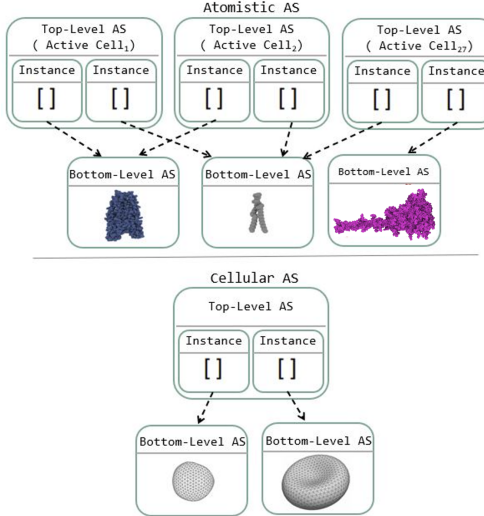


Figure 8: This image shows two types of acceleration structures used by the renderer at the top atomistic AS, which contains the atomistic scale description. The atomistic AS contains several TLASes, a TLAS per active cell. Every TLAS has several instances that point to one of BLASes. At the bottom is the cellular AS, which contains only one TLAS representing the skeleton of the scene.

with a box-tile b . The box tiles $b \in B$ are tiled inside the cells to fill the internal space of the mesh. Analogously to the membrane population, we use the highest number of elements within tile $tileB_{max}$ together with the number of box-tiles fill the cell c , (rep_x, rep_y, rep_z) , calculated as $rep_{xyz} = ceil(size(c)/size(b))$. The number of threads per c is calculated as a product $tileB_{max} \times rep_x \times rep_y \times rep_z$. Threads are associated with a molecular instance m which are stored in a linear buffer of the box-tile b . Few remaining threads are again discontinued. For every instance in a box-tile $m = b[i]$, its relative 3D position inside the box is computed. To calculate the absolute position, we need to calculate the world space position of the starting corner of the box-tile b . This position is calculated from the starting corner of the cell c , the three indices x, y, z that refer to the respective box-tile b and the world-space size of the box-tile $size(b)$. Once the 3D position pos of molecular instance m is calculated, it is tested whether it lies inside the cell c . Moreover, if the cell is intersected by triangles I_c , the algorithm decides on which half-space with the respect to I_c the position pos is. This orientation is determined based on the normal vector of the triangle mesh, whether the normal points toward the pos wrt. the triangle center or away from pos . If pos lies outside the biological structure, it is rejected and the computation stops. In the other case, a new molecular instance m is created based on the information from m_{ref} and its position is set to $m.pos = pos$. For the case when there is no intersection with any mesh in any of $c \in C$, the closest triangle information $c.closestTriangle$ is used as an indicator, and the triangle normal of the closest triangle is again used to determine whether the entire cell cache is inside or outside of the biological structure defined by the mesh. In case it is marked as outside, no population is performed.

7 NanoView: Parallel RTX-based Molecular Rendering

Computational complexity of interactive ray tracing grows logarithmically with the complexity of the scene, which challenges the predominant role of rasterization in complex environments [45–47]. Recent graphics card architectures support hardware accelerated ray tracing. We utilize this new technology to accelerate the rendering of our on-the-fly populated scene.

7.1 Acceleration Structures

The acceleration structure (AS) is a core component of every efficient raytracing algorithm. To accelerate the raytracing in the modern GPUs, this component is implemented in hardware. NVIDIA GPU hardware implementation exposes only two levels of acceleration structure to the user. The *bottom-level AS (BLAS)* defines the geometric description of a molecular model (i.e., the position and radius of its atoms), while the *top-level AS (TLAS)* consists of instances that reference to one of the BLASes [48]. Each instance is associated with the transformation matrix, as well as molecular type of the instance to fetch the corresponding color value. This two-level hierarchy allows us to populate multiple instances of an object, while storing its geometry only once in the GPU memory.

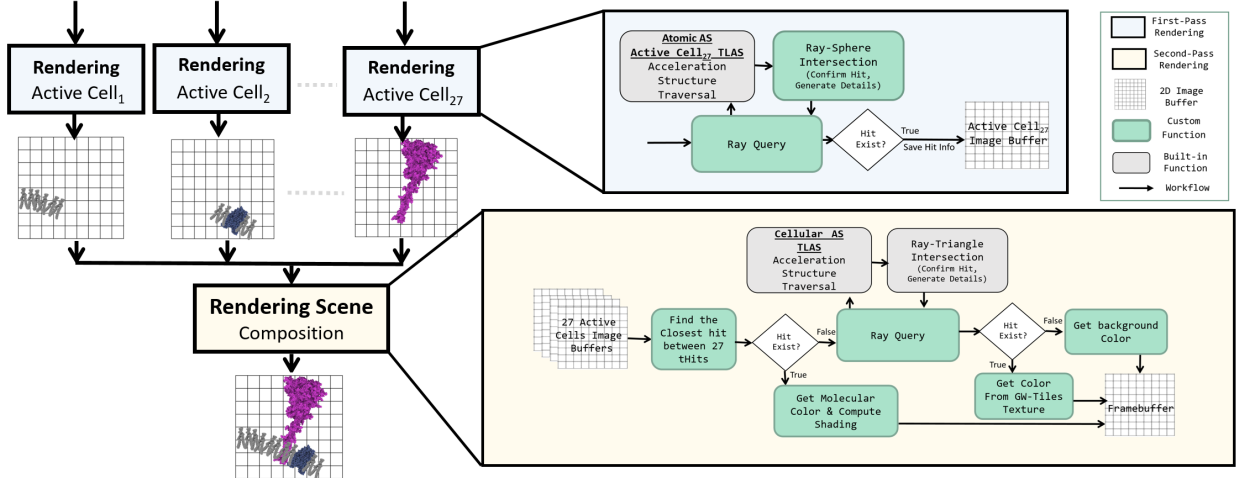


Figure 9: Overview of the parallel rendering pipeline. On the left side, the "sort-last" scheme of parallel rendering is presented which consists of two-pass. The first pass is highlighted with blue boxes that trace the Atomistic AS TLASes in parallel while the yellow box represents the second pass that composites the 27 image buffers. On the right side, corresponding high-level description of each pass.

In our rendering algorithm, we are using two representations of acceleration structures: the *cellular AS*, which defines the skeleton of the scene and contains all the mesh instances that define the shape, size, and position of the biological structures, and *atomistic AS* which contains the atomistic description of the active cells. In cellular AS we create a BLAS for every mesh, while in atomistic AS we create a BLAS for every molecular model and then we instantiate them within the scene (see Figure 8).

Representing the atomistic AS as a single TLAS will lead to rebuilding it from scratch whenever the active cells are changed. RTX acceleration structure allows updating TLAS, which is cheaper than rebuild it, however, it can be used only for updating the instances information e.g. transformation matrix. If a new instance needs to be added to the scene, the TLAS has to be rebuilt. To avoid that, our atomistic AS contains multiple TLASes, one TLAS per active cell. The active cell's TLAS is generated based on the contents of its cache. Once a cell becomes active, its TLAS will be built and will not change until that cell becomes inactive.

For each AS, hardware acceleration requires to provide the type of ray intersection test needed by the traversal program. The selection should be based on the BLAS lowest geometric representation. In the *cellular AS*, the meshes are defined as triangles, therefore we use the hardware triangle-ray intersection test that is built-in in the GPU. In the *atomistic AS* the molecular models are defined through its as atoms/spheres, therefore we use a custom-implemented sphere-ray intersection test.

7.2 Parallel Rendering

The scene is rendered as a combination of atomistic and cellular rendering. Details closer to the camera are rendered at the atomistic resolution, while objects further away from the camera are rendered as textures. To prevent the sudden popping of atomistic structures, we implement a smooth transition from texture details into atomistic details and vice-versa using alpha blending. In the molecular details rendering, the scene is rendered in two-pass rendering. In the first pass, the active cells are rendered separately into their respective frame buffer objects (FBOs). This pass takes the advantage of having multiple TLASes in the atomistic AS to parallelize their rendering. We use the *sort-last* parallel rendering scheme [33] that can render the atomistic AS TLASes in parallel, which results in a very high data rate as the rendering operates independently. But instead of parallelizing the rendering through multiple GPUs, we use one GPU that use compute shader and Nvidia's `GLSL_EXT_ray_query` extension to parallelize the rendering tasks between threads. The ray query extension allows us to invoke ray tracing query through the compute shader. This extension is an alternative to the ray tracing pipeline, but no separate dynamic shader or shader binding table is needed [49]. In the first rendering pass, the atomistic AS TLASes are traced in parallel, a thread per pixel per active cell. In each thread, once the closest hit is found, its information (e.g. depth, instance_id, atom_id) is stored on full screen image buffer of the thread's active cell. Otherwise, the value (-1) is stored which means the ray did not hit any nanoscale structure (see Figure 9).

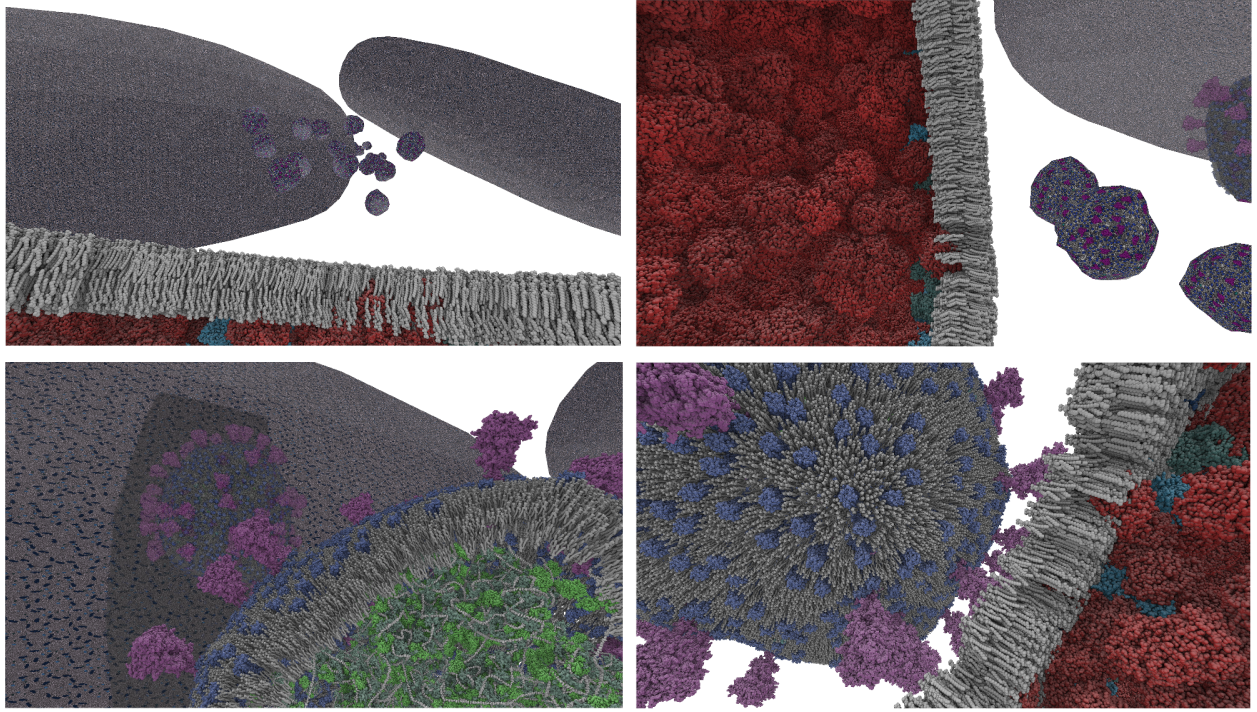


Figure 10: Example of the resulting scene rendered using our RTX pipeline. Top-Left: partially populated RBC membrane with an overview of the scene. Top-Right: View from the populated RBC membrane towards partially populated and not populated SARS-CoV-2 particles. Bottom-Left: View inside SARS-CoV-2 particle. Bottom-Right: View from inside populated RBC towards populated SARS-CoV-2.

In the second pass, the resulting FBOs are composited, based on the depth values to form the final rendered image. If there is at least one hit found in the 27 images, the *instance_id* and *atom_id* of the closest hit among them is used to get the molecular color. In addition, the shading is computed using *phong illumination model* as well as *ray-traced ambient occlusion*. If there is no hit (no nanoscale structure information is found), the cellular structure information is provided using image-based approach.

7.3 Image-based Tiling

Image-based impostors are usually used to avoid rendering objects that are far away from the viewpoint by replacing the geometry of these objects with a painted texture [50–52]. In the tile preparation phase (see subsection 4.2), GW-tiles have been created. Moreover, the corresponding texture map was synthesized. The key idea is to use both of these levels of detail representations, while rendering the scene. When the camera is closer to a biological structure, the GW-tile is used. Once the camera zooms out, which causes the atomistic detail to disappear, the corresponding part of the texture map is rendered in the very same place. In subsection 4.2 also the description of tile recipe TR was presented. The tile recipe forms a virtual map of tiles that covers the whole uv -texture space associated with the mesh.

The texture map is sampled while rendering a cellular mesh using the following approach. Using the texture coordinate uv of a fragment, the respective $tileId$ is obtained from the tiles recipe. Moreover, the relative position rel_{uv} inside this tile is computed. Based on the $tileId$, its respective starting position $tile_{origin}$ in texture map is obtained. The resulting color is fetched for the position $tile_{origin} + rel_{uv}$. Besides the diffuse color, texture map consists of normal and ambient occlusion buffers which are used to add geometric detail to the shaded surface.

To avoid the sharp transition from geometry to image-based representation we apply alpha blending on the instances that are located in the far border of the neighboring cells which combines the geometry atomistic color with image-based cellular color.

8 Results

Our novel construction approach is capable of instantly generating and visualizing biological worlds of cellular mesoscale. We demonstrate the scalability of Nanomatrix on a scene containing a red blood cell and a SARS-CoV-2 virion, as shown in Fig 1.

Instantly generating and rendering such a large scene in atomistic detail was not possible with previous methods. The bounding box size of RBC mesh is $64,360 \times 15,110 \times 75,410 = 73,334,686,636,000 \text{ \AA}^3$. The generated box-tile size is $1,000 \times 1,000 \times 1,000 = 1,000,000,000 \text{ \AA}^3$. Each box-tile has approx. 5,000 molecular instances (hemoglobins of approx 4380 of atoms), with approx. 21,000,000 atoms. Once the RBC would be fully generated, the entire scene would contain approx. 250 millions of molecules with 1.1 trillion of atoms. Additionally, the surface area of the red blood cell (RBC) mesh is $9.54061e + 09 \text{ \AA}^2$. The area of its membrane GW-tile is $500 \times 500 = 250,000 \text{ \AA}^2$. Each membrane GW-tile has approx. 5,000 molecular instances with approx 335,000 atoms. Therefore, the fully populated surface would consist of approx. 175 million of molecular instances with approx. 13 billion of atoms. One SARS-CoV-2 virions consists of approx. 135 thousand molecular instances with approx. 24 million of atoms. In our model scene, there are four RBC and twenty SARS-CoV-2 particles which leads to approx. 5 trillion of atoms in total. However, the algorithm is scalable enough to work with any number of non-overlapping models that can be fitted into the bounding box of the scene.

The implementation of the approach was realized using the Vulkan API [53] and NVIDIA’s nvpro-samples framework [54]. The performance was measured using a NVIDIA GeForce RTX 3090 graphics card with 24 GB memory. In our experiment, we create a grid of dimension $200 \times 200 \times 200$ with cell size 2000. Each cell cache buffer has a room for 1,000,000 molecular instances. These are programmatically adjustable, they can be set to meet the requirements of any dedicated GPU. The construction algorithm is able to populate a cell with the membrane molecules in approx. 6 ms and with solubles molecular in approx. 3 ms. We implemented the approach in two environments. The first environment, where the rendering is built on top of the Marion library, is developed using C++ and OpenGL 4.6 graphics API [55]. The second environment, we call it NanoView, is built using the Vulkan graphics API with RTX functionality. Whereas the construction algorithm has approx. the same performance (as in both cases it relies on the compute shader pipeline and not on the graphics pipeline), the rendering differs significantly. We were able to achieve on average 2.5x speedup from the NanoView framework. On NVIDIA GeForce 3090 in Full HD resolution with similar settings of the scalable construction algorithm, Marion rendering runs at approx. 45 FPS (with drops down to 25 FPS). The NanoView framework runs at approx. 110 FPS (with drops to 80 FPS) with a single ray per pixel and 80 FPS (with drops to 30 FPS) with 5 rays per pixel. This speedup is sufficient enough to provide us with the future possibility of integrating a VR or AR interface, where a high framerate is the key factor for a satisfactory user experience. The performance of Nanomatrix can be further boosted by submitting the rendering and construction workloads into two different *Queue Families* in the GPU which allows the RT Core and compute workloads to be processed concurrently. This is a new feature that is supported by the recent NVIDIA’s graphics card architectures [56].

9 Discussion

We implement Object-Space AO (OSAO) to convey the shape and the depth of molecules by tracing random AO-ray against the TLAS of the active cell to which the hit primitive belongs. The AO algorithm is implemented as described in NVIDIA Vulkan API tutorials [57]. Due to our gridding approach, the AO is inaccurate on the primitives that are located on the borders of active cells. To estimate the shading value correctly, the TLAS of the adjacent cell would need to be traced as well. This is one of the drawbacks of the sort-last scheme of parallel rendering [58]. To overcome this issue, a test has been added in the AO computation, if the hit atom is located on the cell border, then the AO-ray will traverse the AS of all active cells that intersect the hit atom.

The instance count at RTX acceleration structure must not exceed a specific limit which varies based on the graphics card. Our RTX 3090 graphics card supports a maximum 16M instances. However, the scalability of nanomatrix allows overcoming that limit by rendering multiple acceleration structures in parallel. Our method is scalable, however, its parameters should be adjusted based on the available computational resources. As the size increases, more geometrical information will be presented which enriches the scene with detail information. However, it will increase the computational complexity and the memory footprint. Our method allocates a part of the dedicated GPU memory for the cells’ cache buffers. Clearly, increasing the cache buffer size will increase the allocated portion of the memory. On the other hand, increasing the size of the activation window will increase the number of the cells’ cache buffers. In addition, the rendering overhead increases with the size of the activation window, because it requires more rendering threads in the first pass rendering and more images to be composited in the second pass rendering.

Our construction algorithm is meant for explanatory visualization of extremely large cellular mesoscale scenes that can be explored down to atomistic detail. The tiling strategy that we employ may be criticised by repetitiveness and associated plausibility of the resulting model. We want to emphasize that the explanatory visualization scenario allows for a certain algorithmic flexibility that might or might not be acceptable within scientific discovery workflows.

10 Conclusions

This work presents a scalable approach for exploring cellular mesoscale down to their atomistic resolution. We introduce a view-guided construction algorithm based on the Wang Tile concept, both for membrane structures as well as for the internal parts of biological entities. The overall performance is interactive even for hundreds of billions of atoms. Currently, the box-tiling is not aperiodic as the seams are not critical. However, in case we include the representation of linear strands of genetic macromolecules or other fibers, the continuity will become a clear requirement. As the approach which is used for rectangular tiling can be extended for 3D, we can include the fibrous structures as parts of the GW-tiles. If such approach would significantly increase the GPU memory requirements, an on-the-fly fiber population within active cells can be integrated building on the top of Klein et al. parallel fiber generation approach [25]. The new active cells will need to populate the fiber from its last position from previous active cells.

Acknowledgment

The research was supported by the King Abdullah University of Science and Technology (BAS/1/1680-01-01) and KAUST Visualization Core Lab. We thank nanographics.at for providing the Marion library.

References

- [1] David S. Goodsell, Arthur J. Olson, and Stefano Forli. Art and science of the cellular mesoscale. *Trends in Biochemical Sciences*, 45(6):472–483, 2020.
- [2] William Humphrey, Andrew Dalke, and Klaus Schulten. VMD: Visual molecular dynamics. *Journal of Molecular Graphics*, 14(1):33–38, 1996.
- [3] David Sehnal, Sebastian Bittrich, Mandar Deshpande, Radka Svobodová, Karel Berka, Václav Bazgier, Sameer Velankar, Stephen K Burley, Jaroslav Koča, and Alexander S Rose. Mol* Viewer: modern web app for 3D visualization and analysis of large biomolecular structures. *Nucleic Acids Research*, 49(W1):W431–W437, 05 2021.
- [4] Schrödinger, LLC. The PyMOL Molecular Graphics System, Version 1.8. November 2015.
- [5] Aaron Knoll, Ingo Wald, Paul A. Navrátil, Michael E. Papka, and Kelly P. Gaither. Ray tracing and volume rendering large molecular data on multi-core and many-core architectures. In *Proceedings of the 8th International Workshop on Ultrascale Visualization, UltraVis '13*, New York, NY, USA, 2013. Association for Computing Machinery.
- [6] Amira. [Online].
- [7] Thomas Waltemate, Björn Sommer, and Mario Botsch. Membrane Mapping: Combining Mesoscopic and Molecular Cell Visualization. In *Eurographics Workshop on Visual Computing for Biology and Medicine*, 2014.
- [8] Sebastian Grottel, Michael Krone, Christoph Müller, Guido Reina, and Thomas Ertl. MegaMol—A Prototyping Framework for Particle-Based Visualization. *IEEE Transactions on Visualization and Computer Graphics*, 21(2):201–214, 2015.
- [9] Mohamed Ibrahim, Peter Rautek, Guido Reina, Marco Agus, and Markus Hadwiger. Probabilistic Occlusion Culling using Confidence Maps for High-Quality Rendering of Large Particle Data. *IEEE Transactions on Visualization and Computer Graphics (Proceedings IEEE VIS 2021)*, 28(1):573–582, 2022.
- [10] N. Lindow, D. Baum, and H.-C. Hege. Interactive Rendering of Materials and Biological Structures on Atomic and Nanoscopic Scale. *Comput. Graph. Forum*, 31(3pt4):1325–1334, jun 2012.
- [11] Martin Falk, Michael Krone, and Thomas Ertl. Atomistic Visualization of Mesoscopic Whole-Cell Simulations Using Ray-Casted Instancing. *Computer Graphics Forum*, 32, 2013.
- [12] Mathieu Le Muzic, Julius Parulek, Anne-Kristin Stavrum, and Ivan Viola. Illustrative Visualization of Molecular Reactions using Omnipotent Intelligence and Passive Agents. *Computer Graphics Forum*, 33(3):141–150, June 2014. Article first published online: 12 JUL 2014.

- [13] Mathieu Le Muzic, Ludovic Autin, Július Parulek, and Ivan Viola. cellVIEW: a Tool for Illustrative and Multi-Scale Rendering of Large Biomolecular Datasets. *Eurographics Workshop on Visual Computing for Biomedicine*, 2015:61–70, 2015.
- [14] Marco Tarini, Paolo Cignoni, and Claudio Montani. Ambient occlusion and edge cueing for enhancing real time molecular visualization. *IEEE Transactions on Visualization and Computer Graphics*, 12(5):1237–1244, 2006.
- [15] Élie Michel and Tamy Boubekeur. Real time multiscale rendering of dense dynamic stackings. *Computer Graphics Forum*, 39(7):169–179, 2020.
- [16] Paul Merrell and Dinesh Manocha. Model synthesis: A general procedural modeling algorithm. *IEEE transactions on visualization and computer graphics*, 17(6):715–728, 2010.
- [17] Peter Wonka, Michael Wimmer, François Sillion, and William Ribarsky. Instant architecture. *ACM Transactions on Graphics (TOG)*, 22(3):669–677, 2003.
- [18] Stefan Greuter, Jeremy Parker, Nigel Stewart, and Geoff Leach. Real-time procedural generation of 'pseudo infinite' cities. In *Proceedings of the 1st international conference on Computer graphics and interactive techniques in Australasia and South East Asia*, pages 87–ff, 2003.
- [19] Philippe Decaudin and Fabrice Neyret. Rendering forest scenes in real-time. In *EGR04: 15th Eurographics Symposium on Rendering*, pages 93–102. Eurographics Association, 2004.
- [20] Pedro Boechat, Mark Dokter, Michael Kenzel, Hans-Peter Seidel, Dieter Schmalstieg, and Markus Steinberger. Representing and scheduling procedural generation using operator graphs. *ACM Transactions on Graphics (TOG)*, 35(6):1–12, 2016.
- [21] Markus Steinberger, Michael Kenzel, Bernhard Kainz, Peter Wonka, and Dieter Schmalstieg. On-the-fly generation and rendering of infinite cities on the GPU. *Computer Graphics Forum*, 33(2):105–114, 2014.
- [22] Adam Gardner, Ludovic Autin, Brett Barbaro, Arthur J. Olson, and David S. Goodsell. CellPAINT: Interactive Illustration of Dynamic Mesoscale Cellular Environments. *IEEE Computer Graphics and Applications*, 38(6):51–66, 2018.
- [23] Ngan Nguyen, Ondřej Strnad, Tobias Klein, Deng Luo, Ruwayda Alharbi, Peter Wonka, Martina Maritan, Peter Mindek, Ludovic Autin, David S. Goodsell, and Ivan Viola. *italic;modeling in the time of covid-19;/italic;* statistical and rule-based mesoscale models. *IEEE Transactions on Visualization and Computer Graphics*, 27(2):722–732, 2021.
- [24] Graham T. Johnson, Ludovic Autin, Mostafa Al-alusi, David S. Goodsell, Michel F. Sanner, and Arthur J. Olson. cellpack: a virtual mesoscope to model and visualize structural systems biology. *Nature Methods*, 12(1):85–91, 01 2015. Copyright - Copyright Nature Publishing Group Jan 2015; Document feature - ; Last updated - 2018-11-01.
- [25] Tobias Klein, Peter Mindek, Ludovic Autin, David S. Goodsell, Arthur J. Olson, Eduard Gröller, and Ivan Viola. Parallel generation and visualization of bacterial genome structures. *Computer Graphics Forum*, 38, 2019.
- [26] Tobias Klein, Ludovic Autin, Barbora Kozlíková, David S. Goodsell, Arthur Olson, M. Eduard Gröller, and Ivan Viola. Instant Construction and Visualization of Crowded Biological Environments. *IEEE Transactions on Visualization and Computer Graphics*, 24(1):862–872, 2018.
- [27] Hao Wang. Proving theorems by pattern recognition-II. *Bell Labs Technical Journal*, 40(1):1–41, 1961.
- [28] Chi-Wing Fu and Man-Kang Leung. Texture tiling on arbitrary topological surfaces using Wang tiles. In *Rendering Techniques*, pages 99–104, 2005.
- [29] Li-Yi Wei. Tile-based texture mapping on graphics hardware. In *ACM SIGGRAPH 2004 Sketches*, SIGGRAPH '04, page 67, New York, NY, USA, 2004. Association for Computing Machinery.
- [30] Karel Culík and Jarkko Kari. An aperiodic set of wang cubes. *J. Univers. Comput. Sci.*, 1:675–686, 1995.
- [31] Martin Doškář, Jan Zeman, Daniel Rypl, and Jan Novák. Level-set Based Design of Wang Tiles for Modelling Complex Microstructures. *Computer-Aided Design*, 123:102827, 2020.
- [32] Kurt W Fleischer, David H Laidlaw, Bena L Currin, and Alan H Barr. Cellular texture generation. In *Proceedings of the 22nd annual conference on Computer graphics and interactive techniques*, pages 239–248, 1995.
- [33] S. Molnar, M. Cox, D. Ellsworth, and H. Fuchs. A sorting classification of parallel rendering. *IEEE Computer Graphics and Applications*, 14(4):23–32, 1994.
- [34] Steven Molnar, John Eyles, and John Poulton. PixelFlow: High-Speed Rendering Using Image Composition. In *Proceedings of the 19th Annual Conference on Computer Graphics and Interactive Techniques*, SIGGRAPH '92, page 231–240, New York, NY, USA, 1992. Association for Computing Machinery.

- [35] Stefan Eilemann. Parallel Rendering and Large Data Visualization. *CoRR*, abs/1902.08755, 2019.
- [36] Stefan Zellmann, Nate Morrical, Ingo Wald, and Valerio Pascucci. Finding Efficient Spatial Distributions for Massively Instanced 3-d Models. In Steffen Frey, Jian Huang, and Filip Sadlo, editors, *Eurographics Symposium on Parallel Graphics and Visualization*. The Eurographics Association, 2020.
- [37] G. Varadhan and D. Manocha. Out-of-core rendering of massive geometric environments. In *IEEE Visualization, 2002. VIS 2002.*, pages 69–76, 2002.
- [38] Thomas Funkhouser. Database Management for Interactive Display of Large Architectural Models. In *Proceedings of the Graphics Interface 1996 Conference, May 22-24, 1996, Toronto, Ontario, Canada*, pages 1–8. Canadian Human-Computer Communications Society, May 1996.
- [39] Roland Fraedrich, Jens Schneider, and Rüdiger Westermann. Exploring the Millennium Run - Scalable Rendering of Large-Scale Cosmological Datasets. *IEEE Transactions on Visualization and Computer Graphics*, 15(6):1251–1258, 2009.
- [40] Ingo Wald, Andreas Dietrich, and Philipp Slusallek. An interactive out-of-core rendering framework for visualizing massively complex models. In *ACM SIGGRAPH 2005 Courses, SIGGRAPH '05*, page 17–es, New York, NY, USA, 2005. Association for Computing Machinery.
- [41] Jeffrey Scott Vitter. External memory algorithms. In Gianfranco Bilardi, Giuseppe F. Italiano, Andrea Pietracaprina, and Geppino Pucci, editors, *Algorithms — ESA' 98*, pages 1–25, Berlin, Heidelberg, 1998. Springer Berlin Heidelberg.
- [42] Johanna Beyer, Markus Hadwiger, Jens Schneider, Won-Ki Jeong, and Hanspeter Pfister. Distributed terascale volume visualization using distributed shared virtual memory. In *2011 IEEE Symposium on Large Data Analysis and Visualization*, pages 127–128, 2011.
- [43] Hao Wang. Proving theorems by pattern recognition — ii. *The Bell System Technical Journal*, 40(1):1–41, 1961.
- [44] Ngan Nguyen, Ondřej Strnad, Tobias Klein, Deng Luo, Ruwayda Alharbi, Peter Wonka, Martina Maritan, Peter Mindek, Ludovic Autin, David S. Goodsell, and Ivan Viola. *italic;modeling in the time of covid-19;italic;* statistical and rule-based mesoscale models. *IEEE Transactions on Visualization and Computer Graphics*, 27(2):722–732, 2021.
- [45] Ingo Wald and Philipp Slusallek. State of the Art in Interactive Ray Tracing. In *Eurographics 2001 - STARs*. Eurographics Association, 2001.
- [46] Ingo Wald, Philipp Slusallek, and Carsten Benthin. Interactive Distributed Ray Tracing of Highly Complex Models. In *Proceedings of the 12th Eurographics Conference on Rendering*, EGWR'01, page 277–288, Goslar, DEU, 2001. Eurographics Association.
- [47] Ingo Wald. A Flexible and Scalable Rendering Engine for Interactive 3D Graphics. 2002.
- [48] Eric Haines and Tomas Akenine-Möller, editors. *Ray Tracing Gems*. Apress, 2019. <http://raytracinggems.com>.
- [49] khronos Group. Ray Tracing In Vulkan, 2020. <https://www.khronos.org/blog/ray-tracing-in-vulkan>.
- [50] Daniel G Aliaga and Anselmo Lastra. Automatic image placement to provide a guaranteed frame rate. In *Proceedings of the 26th annual conference on Computer graphics and interactive techniques*, pages 307–316, 1999.
- [51] Daniel G. Aliaga, Jonathan D. Cohen, Andrew T. Wilson, Eric Baker, Hansong Zhang, Carl Erikson, Kenneth E. Hoff, Thomas C. Hudson, Wolfgang Stuerzlinger, Rui Bastos, Mary C. Whitton, Frederick P. Brooks, and Dinesh Manocha. MMR: an interactive massive model rendering system using geometric and image-based acceleration. In *SI3D*, 1999.
- [52] Gernot Schaufler and Wolfgang Stürzlinger. Three dimensional image cache for virtual reality. *Computer Graphics Forum*, 15(3):227–235, Aug 1996. Eurographics '96.
- [53] Khronos Group Inc. Ray Tracing in Vulkan, 2020.
- [54] NVIDIA. Nvpro-core: NVIDIA DesignWorks Samples, Accessed Feb. 23, 2021. <https://github.com/nvpro-samples>.
- [55] Peter Mindek, David Kouřil, Johannes Sorger, Daniel Toloudis, Blair Lyons, Graham Johnson, M. Eduard Gröller, and Ivan Viola. Visualization multi-pipeline for communicating biology. *IEEE Transactions on Visualization and Computer Graphics*, 24(1):883–892, 2018.
- [56] NVIDIA. Ampere GA102 GPU Architecture whitepaper, 2021.

- [57] NVIDIA. G-Buffer and Ambient Occlusion - Tutorial. https://github.com/nvpro-samples/vk_raytracing_tutorial_KHR/tree/master/ray_tracing_ao.
- [58] Andreas Dietrich, Enrico Gobbetti, and Sung-Eui Yoon. Massive-model rendering techniques: A tutorial. *IEEE Computer Graphics and Applications*, 27(6):20–34, 2007.